Highlights

Model order reduction of an electro-quasistatic problem using CLN method

Wei Chen, Thomas Henneron, Stéphane Clénet, Théo Delagnes, Jun Zou

- Application of a Model Order Reduction method, Cauer Ladder Network (CLN) method, to reduce electro-quasistatic (EQS) problems. The CLN method were applied to reduce magneto-quasistatic problems.
- Construction of a reduced model under the form of an equivalent electrical circuit, very useful in practice for the study and the design of the EQS device.
- Derivation of an error estimator to calculate the distance between the solution of Finite Element model and the reduced solution given by the CLN method without solving a Finite Element model.
- Application of the CLN method to study an industrial EQS problem.

Model order reduction of an electro-quasistatic problem using CLN method

Wei Chen[a], Thomas Henneron[a], Stéphane Clénet[a,1,*], Théo Delagnes[b], Jun Zou[c]

[a] *Univ. Lille, Arts et Metiers Institute of Technology, Centrale Lille, Junia, ULR 2697 - L2EP, Lille, 59000, France*
[b] *EDF R&D, ERMES, 7 Boulevard Gaspard Monge, Palaiseau, 91120, France*
[c] *Department of Electrical Engineering, Tsinghua University, Beijing, 100084, China*

Abstract

The Cauer ladder network (CLN) method, as proposed by Kameari et al. (2018), has been extensively studied to construct a reduced model of magneto-quasistatic (MQS) Finite Element (FE) models. In this case, this method enables the construction of an equivalent electrical circuit based on resistances and inductances as well as a reduced basis where the solution of a reduced problem is sought. In this article, we propose to extend the applicability of the CLN method to the development of reduced models for FE electro-quasistatic (EQS) models. It appears that the derivation of the reduction of an EQS model is not similar to the one of an MQS model. After development, the process of reduction using CLN leads to consider two electrical circuits based on the cascade association of resistances and capacitances. Each circuit is associated with a reduced basis constructed by applying the self-adjoint Lanczos method. The reduced solution to the EQS problem is got by first solving the circuit equations to determine the voltages and the currents at the terminals of the resistances and capacitances. Then, the approximated solution of the FE EQS model is got by a linear combination of the vectors of the two reduced bases weighted by the currents (or the voltages) previously calculated. An error estimator is also derived, enabling to calculate the distance between the reduced solution and the FE solution without solving the FE model. The proposed approach has been applied on an industrial application, a resin-impregnated paper bushing, in order to evaluate the accuracy in function of the size of the reduced bases as well as the efficiency in terms of computation time.

Keywords: Cauer Ladder Network method, Model Order Reduction, Finite Element Method, Electro-quasistatic (EQS) problem

1. Introduction

The simulation of electromagnetic fields is of great interest for the study and design of electromagnetic devices. Numerical models based on the Finite Element Method (FEM) [1, 2, 3] have become the standard for the analysis and the design of low-frequency electromagnetic devices. Depending on the frequency range, different problems can be derived from Maxwell's equations

*Corresponding author
[1] E-mail addresses: stephane.clenet@ensam.eu (S. Clénet).

under various assumptions. These assumptions are closely related to the influence of the time variation of electromagnetic fields. These new problems enable to simplify drastically the equations to solve without significantly losing precision. These problems are either quasistatic, the electromagnetic fields still depend on time, or static, the fields depend then only on space. By neglecting the influence of the time variation of the electric flux density, the magneto-quasistatic (MQS) problem can be derived. The MQS problem focuses on applications where the resistive and inductive effects are prominent. This problem is largely considered in the literature because it is well suited to model numerous industrial applications like transformers or rotating electrical machines for example. By neglecting the influence of the time variation of the magnetic flux density, the electro-quasistatic (EQS) problem can be derived [4]. The EQS problem enables to consider the resistive and capacitive effect. This problem is less studied in the literature even though it is of great importance especially for high voltage applications [5].

In real industrial applications, electrical devices are generally of complex shapes which require, when using the Finite Element method, a mesh with a high number of elements. It leads to a huge system of differential-algebraic equations to solve. To account for the dynamics of the device, this system of equations has to be solved numerous times either in the time or frequency domain which leads to a high computational time. Consequently, model order reduction methods which enable to reduce the solving time of the FE model, so-called also full model, are of great interest. Instead of solving the full model, the idea of model order reduction methods is to seek for a solution in a basis of small size compared to the size of the equation system of the FE model. The most common ones are the Proper Orthogonal Decomposition (POD) method coupled with the snapshot method [6, 7, 8, 9], the Krylov subspace method [10, 11], and the Proper Generalized Decomposition (PGD) [12, 13, 14]. The Cauer Ladder Network (CLN) method was originally proposed by Kameari et al. [15], to reduce a 2D vector potential FE formulation to solve a MQS problem [15]. This method is a variant of the Krylov subspace method. The main advantage of this method is that the reduced problem after projection relies on an equivalent electrical circuit. It means that once the reduced basis is built in an offline stage, the online stage consists of solving an electrical circuit based on resistances and inductances. The field distributions in the FE space are then reconstructed from currents flowing through the inductances and voltages at the terminals of the resistances. Using the CLN method, the coupling of other circuits is totally natural, which is of great interest in many applications since the device, modeled by the FE method, is very often electrically connecting to other devices represented also by equivalent circuit. Using the self-adjoint Lanczos method [16], this method has been extended to other formulations for 3D problem, including A $-\varphi$ and A-T [17]. Another interest is that an error estimator has also been introduced in the MQS case to estimate the error of reduction, that is to say the distance between the FE solution and the CLN solution [18].

As mentioned above, the CLN approaches have been originally proposed to reduce a MQS problem. A lot of development has been proposed since then and many applications have been treated showing the great interest of this method in studying industrial problems. The reduction of EQS model has been addressed but we can only mention the application of POD approach [19, 20], PGD approach [21], an information based reduction method [22]. No application of the CLN method has reported in the literature to reduce EQS model.

In this article, we propose an extension of the CLN method to construct reduced models of FE electro-quasistatic (EQS) problems. Using the superposition theorem, we divide the EQS problem into two subproblems. Unlike the standard CLN method, which yields a Padé approximation at 0 Hz, our approach approximates the solution of each subproblem at infinite frequency through variable transformation. The self-adjoint Lanczos method is applied to each subprob-

lem, generating respective reduced bases for projecting the overall problem. It is showed that the coefficients associated with the reduced bases lead to an equivalent circuit equation, composed of resistances and capacitances. Thus, instead of directly solving the reduced problem, we employ the equivalent circuit in both frequency and time domains to determine the terminal voltages and currents. The local field approximation is then got from these coefficients. Furthermore, we propose an extension in the EQS case of the error estimator proposed in the MQS case in the frequency domain.

The proposed method is tested on an industrial application, a resin-impregnated paper (RIP) bushing. Two cases are studied, the healthy case and a default case, when it appears locally an electrical connection between two electrodes because of the aging of the insulating material. The idea is to evaluate the capability of the CLN method to capture a global homogeneous behavior (healthy case) as well as local behaviors due to the default (default case). The global behavior is addressed through a factor, so-called dissipation factor, that is used in practice to evaluate the health state of the bushing. The error estimator is also applied to evaluate the quality of the approximation using the CLN method. The local behavior is evaluated by comparing field distribution obtained with the FE model and the CLN model.

2. CLN EQS

2.1. Electro-quasistatic problem

The EQS model addresses phenomena involving conducting and displacement currents, operating under the assumption that the effect of the time variation of the magnetic flux density is negligible. This allows for a simplification of Maxwell's equations as follows:

$$\begin{cases} \operatorname{div}\left(\mathbf{J} + \frac{\partial \mathbf{D}}{\partial t}\right) = 0 \\ \mathbf{curl}\,\mathbf{E} = \mathbf{0} \end{cases} \tag{1}$$

where $\mathbf{J}$, $\mathbf{D}$, and $\mathbf{E}$ represent the current density, electric flux density and electric field, respectively. We seek for the field distributions on a domain Ω with a boundary Γ.

In the linear case, the material constitutive relationships are given by:

$$\mathbf{J} = \sigma \mathbf{E} \tag{2}$$

$$\mathbf{D} = \varepsilon \mathbf{E} \tag{3}$$

where σ and ε denote the electrical conductivity and the electrical permittivity, respectively. These characteristics depend on the position. Finally, we will assume in the following that the conditions on the boundary Γ are:

$$\begin{cases} \mathbf{E} \times \mathbf{n} = 0 \quad \text{on} \quad \Gamma_{\mathrm{E}} \\ \mathbf{J} \cdot \mathbf{n} = 0 \quad \text{on} \quad \Gamma_{\mathrm{J}} \end{cases} \tag{4}$$

with the two boundaries Γ_{E} and Γ_{J} satisfying $\Gamma_{\mathrm{E}} \cup \Gamma_{\mathrm{J}} = \Gamma$ and $\Gamma_{\mathrm{E}} \cap \Gamma_{\mathrm{J}} = 0$. The boundary Γ_{E} is generally not connected gathering surfaces, so-called electrodes, between which the voltages are imposed by an external circuit. We assume in the following that we have only two electrodes Γ_{E_1} and Γ_{E_2} such that $\Gamma_{\mathrm{E}} = \Gamma_{\mathrm{E}_1} \cup \Gamma_{\mathrm{E}_2}$ (Fig. 1). The voltage between both surfaces is imposed to V. The following development can be generalized to over two electrodes. In that case, the number of source functions to be defined is equal to $n - 1$ with n the number of electrodes.

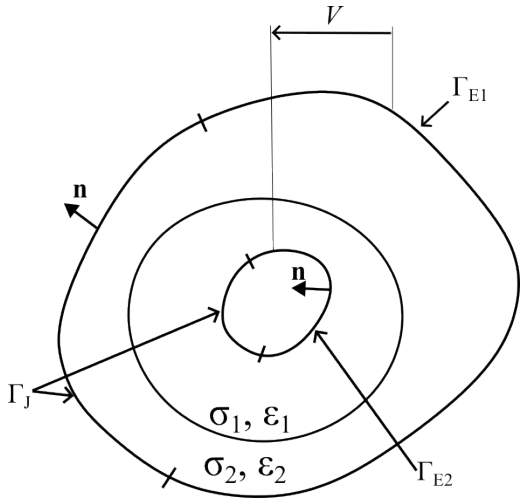

Figure 1: Boundary condition.

2.2. Scalar Potential Representation

To solve the EQS model, the irrational electric field **E** is represented by a scalar potential φ:

$$\mathbf{E} = -\,\mathbf{grad}\,\varphi - V\,\mathbf{grad}\,\alpha \text{ on } \Omega \tag{5}$$

$$\varphi = 0 \text{ on } \Gamma_E \tag{6}$$

where α is a function, which the gradient exists, satisfying:

$$\begin{aligned} \alpha &= 0 \text{ on } \Gamma_{E_1} \\ \alpha &= 1 \text{ on } \Gamma_{E_2} \end{aligned} \tag{7}$$

Substituting **E** in Eq. 1, we obtain the scalar potential formulation:

$$\operatorname{div}\left(\sigma\,\mathbf{grad}\,\varphi + \frac{\partial}{\partial t}(\varepsilon\,\mathbf{grad}\,\varphi)\right) = -\operatorname{div}\left(\sigma V\,\mathbf{grad}\,\alpha + \frac{\partial}{\partial t}(\varepsilon V\,\mathbf{grad}\,\alpha)\right) \tag{8}$$

In the frequency domain, the EQS problem is reformulated as follows:

$$\operatorname{div}\left(\sigma\,\mathbf{grad}\,\varphi + j\omega\varepsilon\,\mathbf{grad}\,\varphi\right) = -\operatorname{div}\left(\sigma V\,\mathbf{grad}\,\alpha + j\omega\varepsilon V\,\mathbf{grad}\,\alpha\right) \tag{9}$$

where ω represents the angular frequency. To discretize this formulation, the Finite Element method (FEM) can be used as explained in the following.

2.3. Variational Formulation

In the FEM framework, the unknown scalar potential φ is represented as a linear combination under the form:

$$\varphi = \sum_{i=1}^{N_n} w_i^0 \varphi_i \tag{10}$$

where w_i^0 represent the nodal interpolation functions and φ_i are coefficients, and N_n the number of unknowns. According to the delta-Kronecker property of the interpolation functions, the coefficient φ_i is equal to the value of the scalar potential φ at the node i. Since the potential value of φ is known and equal to zero on the boundary Γ_{E}, the value of the coefficients φ_i associated with nodes on the boundary Γ_{E} are prescribed to zero. If N_t denotes the total number of nodes and N_c the total number of nodes on the boundary Γ_{E}, then we have the number of unknowns $N_n = N_t - N_c$.

The source function α can be also decomposed under the form:

$$\alpha = \sum_{i=1}^{N_t} w_i^0 \alpha_i \tag{11}$$

with α_i the nodal value of the function α at the node i. A simple way to obtain a function α is to impose the coefficients α_i equal to 1 on the associated nodes located on Γ_{E_2} and equal to zero on the other nodes (see Fig. 2).

Applying the Finite Element Method and the weighted residual method to the EQS formulation yields to the following linear system of equations:

$$\mathbf{N}_{\mathrm{EQS}}\mathbf{X}_\varphi + j\omega\mathbf{K}_{\mathrm{EQS}}\mathbf{X}_\varphi = j\omega V\mathbf{F_1} + V\mathbf{F_2} \tag{12}$$

where $\mathbf{N}_{\mathrm{EQS}}$ and $\mathbf{K}_{\mathrm{EQS}}$ are matrices in $\mathbb{R}^{N_n \times N_n}$, and $\mathbf{X}_\varphi$, $\mathbf{F_1}$, $\mathbf{F_2}$ are vectors in $\mathbb{R}^{N_n}$, defined as:

$$\begin{aligned}
\mathbf{N}_{\mathrm{EQS}} &= [N_{ij}], \quad N_{ij} = \int_\Omega \sigma\, \mathbf{grad}\, w_i^0 \cdot \mathbf{grad}\, w_j^0 d\Omega \\
\mathbf{K}_{\mathrm{EQS}} &= [K_{ij}], \quad K_{ij} = \int_\Omega \varepsilon\, \mathbf{grad}\, w_i^0 \cdot \mathbf{grad}\, w_j^0 d\Omega \\
\mathbf{F_1} &= [F_{1i}], \quad F_{1i} = -\int_\Omega \varepsilon\, \mathbf{grad}\, w_i^0 \cdot \mathbf{grad}\, \alpha d\Omega \\
\mathbf{F_2} &= [F_{2i}], \quad F_{2i} = -\int_\Omega \sigma\, \mathbf{grad}\, w_i^0 \cdot \mathbf{grad}\, \alpha d\Omega \\
\mathbf{X}_\varphi &= [\varphi_i]
\end{aligned} \tag{13}$$

This system of equation is generally large especially in 3D. In order to reduce the number of unknowns of the problem, MOR methods can be applied, like the CLN method. This method has been already used to reduce MQS problem as it will be presented in the following. Then, we will extend the use of the CLN method to reduce the EQS problem just presented before.

2.4. CLN method

The CLN method was originally proposed by the Kameari et al. [15] to reduce MQS problems based on $\mathbf{A}^*$ potential formulation. It is later established that the CLN approach is based on the Lanczos algorithm with respect to a self-adjoint matrix [16] and, making it applicable to matrix systems of a specific form, as described in this subsection.

2.4.1. CLN for MQS problems

We consider a MQS problem illustrated in Fig. 3 with one massive conductor supplied by a current i_{MQS}. In the following, we will show how the CLN method is applied to obtain a reduced

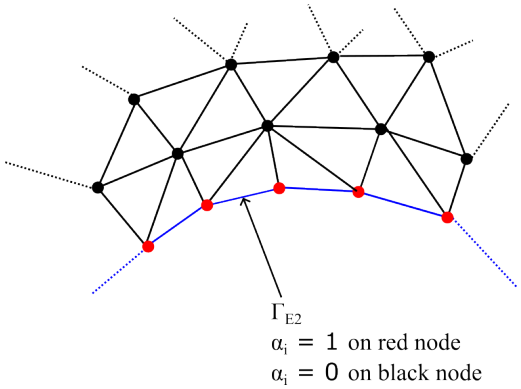

Figure 2: Illustration of node value α_i of α in the FEM framework.

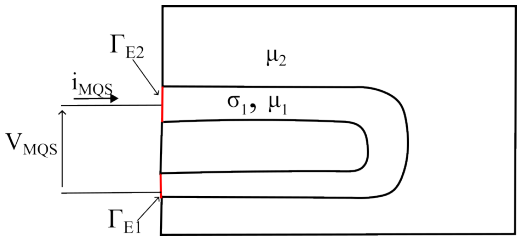

Figure 3: Analysis domain and power supply for MQS problem.

model. To solve the MQS problem, we will consider a modified FEM $\mathbf{A} - \varphi$ formulation where the scalar potential φ has been eliminated as proposed in [16]. The equation system to be solved can be written under the form:

$$\mathbf{Ka} + s\mathbf{Na} = i_{MQS}\mathbf{F} \tag{14}$$

$$s = j\omega \tag{15}$$

where $\mathbf{a}$ is the vector of the coefficients when the vector potential $\mathbf{A}$ is decomposed in the edge element space, $\mathbf{K}$ and $\mathbf{N}$ are matrices associated with magnetic permeability and electrical conductivity respectively and $\mathbf{F}$ is a vector enabling to impose a current i_{MQS} in the massive conductor. This vector is obtained after solving an electrokinetic problem with scalar potential φ on the massive conductor by imposing a current of 1 A. The solution of the electrokinetic problem enables to determine the DC resistance R_0 of the massive conductor.

For a MQS problem, generally the voltage V_{MQS} is imposed instead of the current i_{MQS}. The current becomes then an unknown of the problem and verifies the following equation that is coupled to Eq. 14:

$$R_0 i_{MQS} + s\mathbf{F}^T\mathbf{a} = V_{MQS} \tag{16}$$

To develop the reduced model of the coupled Eq. 14 and Eq. 16, we will first focus on the reduction of Eq. 14. The CLN algorithm (Algorithm 1) is applicable to matrix systems in the form of Eq. 14, provided that $\mathbf{N}$ is a symmetric real matrix, $\mathbf{F}$ is a real vector and $\mathbf{K}$ is symmetric real matrix. The problem is supposed to be compatible that is to say it exists solutions $\mathbf{x}_1, \cdots,$

$\mathbf{x}_{2n+1}$ for equations introduced in the CLN algorithm (Algorithm 1) :

$$\mathbf{K}\mathbf{x}_1 = \mathbf{F} \tag{17}$$

$$\mathbf{K}\mathbf{x}_{2q+1} = \mathbf{N}\mathbf{v}_{2q}\frac{1}{\kappa_{2q}} \tag{18}$$

where $q = [1, n]$ and n is number of stages.

In the case of the formulation introduced in Eq. 14, $\mathbf{K}$ can be singular, and the problem may not be always compatible [23]. However, we assume in the following that the mesh is sufficiently fine so that when applying an iterative method like the conjugate gradient method, we obtain a solution of very good quality so that the Eq. 17 and Eq. 18 are almost satisfied. In the EQS problem that we will consider in the following, the matrix $\mathbf{K}$ is invertible.

The CLN algorithm (Algorithm 1) yields the reduced bases $\mathbf{U}_n = [\mathbf{u}_1, \cdots, \mathbf{u}_{2n-1}]$, $\mathbf{V}_n = [\mathbf{v}_2, \cdots, \mathbf{v}_{2n}]$ and constants $\kappa_1, \cdots, \kappa_{2n+1}$. The dimension n of the reduced basis is directly linked to accuracy of the CLN method. This dimension can be determined from the error estimator introduced in the section 2.5. The vectors $\mathbf{u}_{2q-1}$ and $\mathbf{v}_{2q}$ are orthogonal with respect to the $\mathbf{K}$ and $\mathbf{N}$ inner products, respectively.

$$\forall i, j \in [1, n], \quad \mathbf{u}_{2i-1}^T \mathbf{K}\mathbf{u}_{2j-1} = \kappa_{2i-1}\delta_{i,j} \tag{19}$$

$$\forall i, j \in [1, n], \quad \mathbf{v}_{2i}^T \mathbf{N}\mathbf{v}_{2j} = \kappa_{2i}\delta_{i,j} \tag{20}$$

where $\delta_{i,j}$ is the Kronecker symbol.

The matrices $\mathbf{K}$ and $\mathbf{N}$ are positive in the case of MQS problem. Hence, the values of $\kappa_1, \cdots, \kappa_{2n+1}$ are all non negative. Moreover, the numerical experiments on practical problems show these values are strictly positive, so in the following, we assume they are strictly positive. The matrices $\mathbf{K}$ and $\mathbf{N}$ are positive definite matrices that is to say that their inverse exists and is also positive. In the case of EQS problem, this issue will not appear since the matrix $\mathbf{K}$ is definite positive and the matrix $\mathbf{N}$ is also definite positive for its restriction corresponding to the conductive region.

Algorithm 1 Pseudocode for CLN algorithm [16]

Input: Input data $\mathbf{K}, \mathbf{N}, \mathbf{F}, n$
Solve $\mathbf{K}\mathbf{x}_1 = \mathbf{F}$, set $\mathbf{u}_1 = \mathbf{x}_1$ and compute $k_1 = \mathbf{u}_1^T \mathbf{K}\mathbf{u}_1$
for $q = 1$ **to** n **do**
  Compute $\mathbf{v}_{2q} = \mathbf{v}_{2q-2} + \mathbf{u}_{2q-1}\frac{1}{k_{2q-1}}$
  Compute $k_{2q} = \mathbf{v}_{2q}^T \mathbf{N}\mathbf{v}_{2q}$
  Solve $\mathbf{K}\mathbf{x}_{2q+1} = \mathbf{N}\mathbf{v}_{2q}\frac{1}{k_{2q}}$
  Compute $\mathbf{u}_{2q+1} = \mathbf{u}_{2q-1} - \mathbf{x}_{2q+1}$
  Compute $k_{2q+1} = \mathbf{u}_{2q+1}^T \mathbf{K}\mathbf{u}_{2q+1}$
end for
Return: $\{\mathbf{u}_1, \cdots, \mathbf{u}_{2n+1}\}, \{\mathbf{v}_2, \cdots, \mathbf{v}_{2n}\}, \{k_1, \cdots, k_{2n+1}\}$

It can be noticed that $\mathbf{U}_n$ and $\mathbf{V}_n$ span the same space because of the linear relation see CLN algorithm (Algorithm 1):

$$\mathbf{v}_{2q} = \mathbf{v}_{2q-2} + \mathbf{u}_{2q-1}\frac{1}{\kappa_{2q-1}} \tag{21}$$

An approximation of $\mathbf{a}$ in the space spanned by reduced basis $\mathbf{U}_n$ or $\mathbf{V}_n$ is sought such that:

$$\mathbf{a} \approx \sum_{q=1}^{n} x_{2q-1}\mathbf{u}_{2q-1} = \sum_{q=1}^{n} y_{2q}\mathbf{v}_{2q} \tag{22}$$

where $x_1, \cdots, x_{2n-1}$ and $y_1, \cdots, y_{2n}$ are the coefficients. We can see here that now the number of unknowns of the problem is not related to the number of edges of the mesh N_a as it is when applying the FEM but to the size of the reduced basis n which can be chosen much smaller than N_a.

To derive the relationship between these coefficients, we replace $\mathbf{a}$ by its expression Eq. 22 in Eq. 14 and apply a Galerkin projection. We obtain then the following equation system:

$$\mathbf{U_n}^T\mathbf{K}\sum_{q=1}^{n} x_{2q-1}\mathbf{u}_{2q-1} + s\mathbf{U_n}^T\mathbf{N}\sum_{q=1}^{n} y_{2q}\mathbf{v}_{2q} = i_{MQS}\mathbf{U_n}^T\mathbf{F} \tag{23}$$

The Eq. 23 can be rewritten as:

$$\mathbf{U_n}^T\mathbf{K}\sum_{q=1}^{n} x_{2q-1}\mathbf{u}_{2q-1} = -\mathbf{U_n}^T(s\mathbf{N}\sum_{q=1}^{n} y_{2q}\mathbf{v}_{2q} + i_{MQS}\mathbf{F}) \tag{24}$$

To derive the relationship between coefficients, the following proposition derived from Eq. 17 and Eq. 18 can be used:

$$\begin{aligned} s\mathbf{N}\sum_{q=1}^{n} y_{2q}\mathbf{v}_{2q} - i_{MQS}\mathbf{F} &= s\sum_{q=1}^{n} y_{2q}\mathbf{N}\mathbf{v}_{2q} - i_{MQS}\mathbf{F} \\ &= s\sum_{q=1}^{n} y_{2q}\kappa_{2q}\mathbf{K}(\mathbf{u}_{2q-1} - \mathbf{u}_{2q+1}) - i_{MQS}\mathbf{K}\mathbf{u}_1 \\ &= s\mathbf{K}(\sum_{q=1}^{n} y_{2q}\kappa_{2q}\mathbf{u}_{2q-1} - \sum_{q=2}^{n} y_{2q-2}\kappa_{2q-2}\mathbf{u}_{2q-1} - y_{2n}\kappa_{2n}\mathbf{u}_{2n+1}) - i_{MQS}\mathbf{K}\mathbf{u}_1 \end{aligned} \tag{25}$$

Substitute the left term of Eq. 24 with the Eq. 25:

$$\mathbf{U}^T\mathbf{K}\sum_{q=1}^{n} x_{2q-1}\mathbf{u}_{2q-1} = -s\mathbf{U}^T\mathbf{K}(\sum_{q=1}^{n} y_{2q}\kappa_{2q}\mathbf{u}_{2q-1} - \sum_{q=2}^{n} y_{2q-2}\kappa_{2q-2}\mathbf{u}_{2q-1} - y_{2n}\kappa_{2n}\mathbf{u}_{2n+1} - i_{MQS}\mathbf{u}_1) \tag{26}$$

Using the orthogonality condition of the basis given in Eq. 19, we get the equations:

$$\begin{aligned} x_1 + sy_2\kappa_2 &= i_{MQS} \\ \forall q \in [2, n] \quad x_{2q-1} + s(y_{2q}\kappa_{2q} - y_{2q-2}\kappa_{2q-2}) &= 0 \end{aligned} \tag{27}$$

Moreover, according to Eq. 21, we obtain:

$$\begin{aligned}\sum_{q=1}^{n} y_{2q}\mathbf{v}_{2q} &= \sum_{q=1}^{n} x_{2q-1}\mathbf{u}_{2q-1} \\ &= x_1\kappa_1\mathbf{v}_2 + \sum_{q=2}^{n} x_{2q-1}\kappa_{2q-1}(\mathbf{v}_{2q} - \mathbf{v}_{2q-2}) \\ &= \sum_{q=1}^{n} x_{2q-1}\kappa_{2q-1}\mathbf{v}_{2q} - \sum_{q=1}^{n-1} x_{2q+1}\kappa_{2q+1}\mathbf{v}_{2q} \\ &= \sum_{q=1}^{n-1}(x_{2q-1}\kappa_{2q-1} - x_{2q+1}\kappa_{2q+1})\mathbf{v}_{2q} + x_{2n-1}\kappa_{2n-1}\mathbf{v}_{2n}\end{aligned} \tag{28}$$

The reduced basis $\mathbf{U}_n$ or $\mathbf{V}_n$ are of rank n if there is no rank deficiency during the iteration of CLN algorithm. Thus, the coefficients $x_1, \cdots, x_{2n-1}$ and $y_2, \cdots, y_{2n}$ satisfy:

$$\begin{aligned} y_{2n} &= x_{2n-1}\kappa_{2n-1} \\ \forall q \in [1, n-1] \quad y_{2q} &= (x_{2q-1}\kappa_{2q-1} - x_{2q+1}\kappa_{2q+1}) \end{aligned} \tag{29}$$

Now, we will consider the coupling as described in Eq. 16 by substituting the approximation of **a** from Eq. 22, resulting in:

$$\begin{aligned} R_0 i_{MQS} + s\mathbf{F}^T \sum_{q=1}^{n} x_{2q-1}\mathbf{u}_{2q-1} &= V_{MQS} \\ R_0 i_{MQS} + s(\mathbf{K}\mathbf{u}_1)^T \sum_{q=1}^{n} x_{2q-1}\mathbf{u}_{2q-1} &= V_{MQS} \\ R_0 i_{MQS} + s\mathbf{u}_1^T\mathbf{K} \sum_{q=1}^{n} x_{2q-1}\mathbf{u}_{2q-1} &= V_{MQS} \\ R_0 i_{MQS} + s x_1\kappa_1 &= V_{MQS} \end{aligned} \tag{30}$$

New coefficients $z_2, \cdots, z_{2n}$ are introduced such that:

$$\forall q \in [1, n] \quad z_{2q} = s y_{2q} \tag{31}$$

These coefficients enable to interpret the Eq. 32-33 and Eq. 30 as a set of equations representing Kirchhoff's circuit laws for an equivalent circuit (see Fig. 4). The coefficients $z_2, \cdots, z_{2n}$ verify the following equations:

$$\begin{aligned} x_1 + z_2\kappa_2 &= i_{MQS} \\ \forall q \in [2, n] \quad x_{2q-1} + (z_{2q}\kappa_{2q} - z_{2q-2}\kappa_{2q-2}) &= 0 \end{aligned} \tag{32}$$

$$\begin{aligned} z_{2n} &= s x_{2n-1}\kappa_{2n-1} \\ \forall q \in [1, n-1] \quad z_{2q} &= s(x_{2q-1}\kappa_{2q-1} - x_{2q+1}\kappa_{2q+1}) \end{aligned} \tag{33}$$

In this circuit (Fig. 4), R_0, $\kappa_2, \cdots, \kappa_{2n}$ are the values of resistances, $z_2, \cdots, z_{2n}$ the voltages at the terminals of the resistances, while $\kappa_1, \cdots, \kappa_{2n-1}$ are the values of inductances and $x_1, \cdots, x_{2n-1}$ the currents flowing through the inductances. The value of V_{MQS} is interpreted as the applied source of voltage for the circuit.

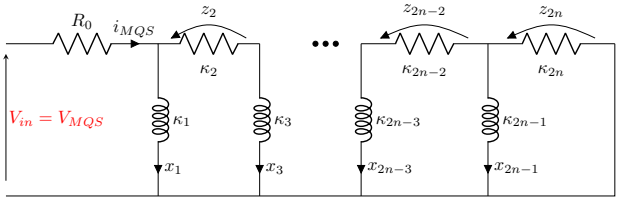

Figure 4: Equivalent circuit for $s = j\omega$ with source of tension V_{MQS}.

2.4.2. *CLN for EQS problem*

For the EQS equation system as described by Eq. 12, the previous method developed in the previous section in the case of MQS cannot be applied directly because of the singularity of the matrix $\mathbf{N}_{\text{EQS}}$, due to the nullity of the conductivity in certain sub-domains. Additionally, the right-hand source is angular frequency-dependent, complicating also the direct application.

Nevertheless, the matrix $\mathbf{K}_{\text{EQS}}$ is always guaranteed to be symmetric and positive definite since the permittivity is strictly positive throughout the entire domain. The EQS equation system can be decomposed into two subsystems of equations:

$$\mathbf{K}_{\text{EQS}}\mathbf{X}_{\mathbf{F_1}} + s\mathbf{N}_{\text{EQS}}\mathbf{X}_{\mathbf{F_1}} = V\mathbf{F_1} \tag{34}$$

$$\mathbf{K}_{\text{EQS}}\mathbf{X}_{\mathbf{F_2}} + s\mathbf{N}_{\text{EQS}}\mathbf{X}_{\mathbf{F_2}} = sV\mathbf{F_2} \tag{35}$$

with $s = \dfrac{1}{j\omega}$. The solution $\mathbf{X}_\varphi$ of the initial equation EQS system can be expressed as:

$$\mathbf{X}_\varphi = \mathbf{X}_{\mathbf{F_1}} + \mathbf{X}_{\mathbf{F_2}} \tag{36}$$

with $\mathbf{X}_{\mathbf{F_1}}$ and $\mathbf{X}_{\mathbf{F_2}}$ the solutions of the two subsystems.

The method presented in the previous section can be applied directly to the two subsystems. In the following we will consider the first subsystem with the source term $V\mathbf{F_1}$. We can proceed in a similar way for the second subsystem with the source term $sV\mathbf{F_2}$. Since the conditions of application of the CLN method described in the previous section are fulfilled, a set of reduced bases and coefficients can be constructed $\{\mathbf{u}_{1,\mathbf{F_1}}, \cdots, \mathbf{u}_{2n-1,\mathbf{F_1}}\}$, $\{\mathbf{v}_{2,\mathbf{F_1}}, \cdots, \mathbf{v}_{2n,\mathbf{F_1}}\}$, $\{k_{1,\mathbf{F_1}}, \cdots, k_{2n,\mathbf{F_1}}\}$.

Applying the interpolation process presented in the previous section with a current source to Eq. 34 allows for the approximation:

$$\mathbf{X}_{\mathbf{F_1}} \approx \mathbf{X}'_{\mathbf{F_1}} = \sum_{q=1}^{n} x_{2q-1,\mathbf{F_1}}\mathbf{u}_{2q-1,\mathbf{F_1}} = \sum_{q=1}^{n} y_{2q,\mathbf{F_1}}\mathbf{v}_{2q,\mathbf{F_1}} \tag{37}$$

This yields a set of equations that are satisfied by the coefficients $x_{1,\mathbf{F_1}}, \cdots, x_{2n-1,\mathbf{F_1}}$ and $y_{2,\mathbf{F_1}}, \cdots, y_{2n,\mathbf{F_1}}$:

$$\begin{aligned} x_{1,\mathbf{F_1}} + sy_{2,\mathbf{F_1}}\kappa_{2,\mathbf{F_1}} &= V \\ \forall q \in [2,n] \quad x_{2q-1,\mathbf{F_1}} + s(y_{2q,\mathbf{F_1}}\kappa_{2q,\mathbf{F_1}} - y_{2q-2,\mathbf{F_1}}\kappa_{2q-2,\mathbf{F_1}}) &= 0 \end{aligned} \tag{38}$$

$$\begin{aligned} y_{2n,\mathbf{F_1}} &= x_{2n-1,\mathbf{F_1}}\kappa_{2n-1,\mathbf{F_1}} \\ \forall q \in [1,n-1] \quad y_{2q,\mathbf{F_1}} &= (x_{2q-1,\mathbf{F_1}}\kappa_{2q-1,\mathbf{F_1}} - x_{2q+1,\mathbf{F_1}}\kappa_{2q+1,\mathbf{F_1}}) \end{aligned} \tag{39}$$

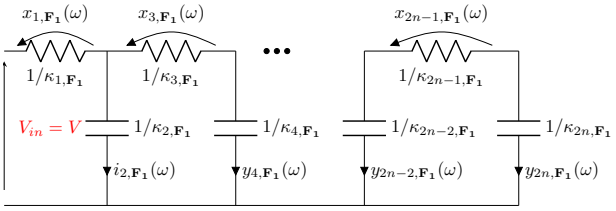

Figure 5: Equivalent circuit for source term $V\mathbf{F_1}$ with source of tension V.

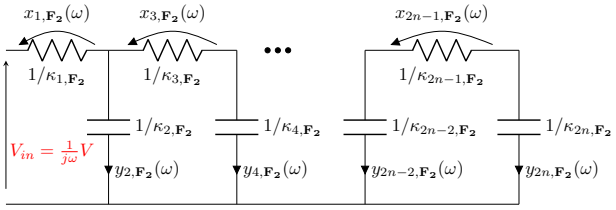

Figure 6: Equivalent circuit for source term $sV\mathbf{F_2}$ with source of tension $\frac{1}{j\omega}V$.

These equations, depicted in Eq. 38 and Eq. 39, can be interpreted as the Kirchhoff's circuit laws of circuit. An equivalent circuit can be deduced presented in Fig. 5, where $1/\kappa_{1,\mathbf{F_1}}, \cdots, 1/\kappa_{2n-1,\mathbf{F_1}}$ represent resistances, $x_{1,\mathbf{F_1}}, \cdots, x_{2n-1,\mathbf{F_1}}$ the voltages, $1/\kappa_{2,\mathbf{F_1}}, \cdots, 1/\kappa_{2n,\mathbf{F_1}}$ the capacitances, and $y_{2,\mathbf{F_1}}, \cdots, y_{2n,\mathbf{F_1}}$ the currents. The value of V is the applied voltage source.

A similar process is applied to the equation 35 with the source term $sV\mathbf{F_2}$, leading to the equivalent circuit in Fig. 6.

$$\mathbf{X}_{\mathbf{F_2}} \approx \mathbf{X}'_{\mathbf{F_2}} = \sum_{q=1}^{n} x_{2q-1,\mathbf{F_2}}\mathbf{u}_{2q-1,\mathbf{F_2}} = \sum_{q=1}^{n} y_{2q,\mathbf{F_2}}\mathbf{v}_{2q,\mathbf{F_2}} \tag{40}$$

Once the two equivalent circuits are determined during an offline stage described above. An approximation $\mathbf{X}'_{\varphi}$ of the solution of the initial equation EQS system can be obtained by summing up the two approximations $\mathbf{X}'_{\mathbf{F_1}}$ and $\mathbf{X}'_{\mathbf{F_2}}$ obtained after the solution of the two circuits (see Fig. 5 and Fig. 6) and the expressions 37 and 40.

2.5. Error Estimator

The vector $\mathbf{X}'_{\mathbf{F_1}}$ obtained with the CLN method is an approximation of the solution $\mathbf{X}_{\mathbf{F_1}}$ of the FE problem 34. In the following, we derive an error estimator enabling to calculate the distance between the approximation $\mathbf{X}'_{\mathbf{F_1}}$ and the FE solution $\mathbf{X}_{\mathbf{F_1}}$. This error estimator in the EQS case has been derived from one proposed in the case of MQS [18].

To derive this error estimator, we construct an auxiliary solution $\mathbf{X}''_{\mathbf{F_1}}$:

$$\mathbf{X}''_{\mathbf{F_1}} = \mathbf{X}'_{\mathbf{F_1}} + sy_{2n,\mathbf{F_1}}\kappa_{2n,\mathbf{F_1}}\mathbf{u}_{2n+1,\mathbf{F_1}} \tag{41}$$

Using Eq. 25, the auxiliary approximation $\mathbf{X}''_{\mathbf{F_1}}$ satisfies:

$$\mathbf{K}_{\mathrm{EQS}}\mathbf{X}''_{\mathbf{F_1}} = -s\mathbf{N}_{\mathrm{EQS}}\mathbf{X}'_{\mathbf{F_1}} + V\mathbf{F_1} \tag{42}$$

The error estimator $\epsilon^2_{\mathbf{K},\mathbf{F}_1}$ satisfies:

$$\begin{aligned}\epsilon^2_{\mathbf{K},\mathbf{F}_1} &= \left\|\mathbf{X}''_{\mathbf{F}_1} - \mathbf{X}'_{\mathbf{F}_1}\right\|^2_{\mathbf{K}} \\ &= \left\|\mathbf{X}''_{\mathbf{F}_1} - \mathbf{X}_{\mathbf{F}_1} + \mathbf{X}_{\mathbf{F}_1} - \mathbf{X}'_{\mathbf{F}_1}\right\|^2_{\mathbf{K}} \\ &= \left\|\mathbf{X}''_{\mathbf{F}_1} - \mathbf{X}_{\mathbf{F}_1}\right\|^2_{\mathbf{K}} + \left\|\mathbf{X}_{\mathbf{F}_1} - \mathbf{X}'_{\mathbf{F}_1}\right\|^2_{\mathbf{K}} \\ &+ (\mathbf{X}''_{\mathbf{F}_1} - \mathbf{X}_{\mathbf{F}_1})^{\mathrm{H}}\mathbf{K}_{\mathrm{EQS}}(\mathbf{X}_{\mathbf{F}_1} - \mathbf{X}'_{\mathbf{F}_1}) + (\mathbf{X}_{\mathbf{F}_1} - \mathbf{X}'_{\mathbf{F}_1})^{\mathrm{H}}\mathbf{K}_{\mathrm{EQS}}(\mathbf{X}''_{\mathbf{F}_1} - \mathbf{X}_{\mathbf{F}_1})\end{aligned} \tag{43}$$

where the norms are defined as follow $\left\|\mathbf{X}_{\mathbf{F}_1}\right\|^2_{\mathbf{K}} = {\mathbf{X}_{\mathbf{F}_1}}^{\mathrm{H}}\mathbf{K}_{\mathrm{EQS}}\mathbf{X}_{\mathbf{F}_1}$, $\left\|\mathbf{X}_{\mathbf{F}_1}\right\|^2_{\mathbf{N}} = {\mathbf{X}_{\mathbf{F}_1}}^{\mathrm{H}}\mathbf{N}_{\mathrm{EQS}}\mathbf{X}_{\mathbf{F}_1}$ and ${\mathbf{X}_{\mathbf{F}_1}}^{\mathrm{H}}$ denotes the Hermitian transpose of $\mathbf{X}_{\mathbf{F}_1}$. According to the expressions 42 and 34, we can show that:

$$\begin{aligned}\mathbf{K}_{\mathrm{EQS}}(\mathbf{X}''_{\mathbf{F}_1} - \mathbf{X}_{\mathbf{F}_1}) &= -s\mathbf{N}_{\mathrm{EQS}}\mathbf{X}'_{\mathbf{F}_1} + V\mathbf{F_1} - (-s\mathbf{N}_{\mathrm{EQS}}\mathbf{X}_{\mathbf{F}_1} + V\mathbf{F_1}) \\ &= -s\mathbf{N}_{\mathrm{EQS}}(\mathbf{X}'_{\mathbf{F}_1} - \mathbf{X}_{\mathbf{F}_1})\end{aligned} \tag{44}$$

The error estimator $\epsilon^2_{\mathbf{K},\mathbf{F}_1}$ satisfied the following relation:

$$\begin{aligned}\epsilon^2_{\mathbf{K},\mathbf{F}_1} &= \left\|\mathbf{X}''_{\mathbf{F}_1} - \mathbf{X}_{\mathbf{F}_1}\right\|^2_{\mathbf{K}} + \left\|\mathbf{X}_{\mathbf{F}_1} - \mathbf{X}'_{\mathbf{F}_1}\right\|^2_{\mathbf{K}} - s\left\|\mathbf{X}_{\mathbf{F}_1} - \mathbf{X}'_{\mathbf{F}_1}\right\|^2_{\mathbf{N}} + s\left\|\mathbf{X}_{\mathbf{F}_1} - \mathbf{X}'_{\mathbf{F}_1}\right\|^2_{\mathbf{N}} \\ &= \left\|\mathbf{X}''_{\mathbf{F}_1} - \mathbf{X}_{\mathbf{F}_1}\right\|^2_{\mathbf{K}} + \left\|\mathbf{X}_{\mathbf{F}_1} - \mathbf{X}'_{\mathbf{F}_1}\right\|^2_{\mathbf{K}} \geq \left\|\mathbf{X}_{\mathbf{F}_1} - \mathbf{X}'_{\mathbf{F}_1}\right\|^2_{\mathbf{K}}\end{aligned} \tag{45}$$

We can show that there is a link between the error estimator and the distance between the CLN solutions $\mathbf{X}'_{\mathbf{F}_1}$ and $\mathbf{X}''_{\mathbf{F}_1}$ and the FE solution $\mathbf{X}_{\mathbf{F}_1}$. The error estimator which can easily calculated from the approximation given by the CLN method is a bound of the term $\left\|\mathbf{X}'_{\mathbf{F}_1} - \mathbf{X}_{\mathbf{F}_1}\right\|^2_{\mathbf{K}}$ which is the distance between the approximation $\mathbf{X}'_{\mathbf{F}_1}$ and the FE solution $\mathbf{X}_{\mathbf{F}_1}$. This bound can be obtained without any FE solution.

Similarly, the error estimator $\epsilon^2_{\mathbf{K},\mathbf{F}_2}$ is derived:

$$\begin{aligned}\epsilon^2_{\mathbf{K},\mathbf{F}_2} &= \left\|\mathbf{X}''_{\mathbf{F}_2} - \mathbf{X}'_{\mathbf{F}_2}\right\|^2_{\mathbf{K}} \\ &= \left\|\mathbf{X}''_{\mathbf{F}_2} - \mathbf{X}_{\mathbf{F}_2} + \mathbf{X}_{\mathbf{F}_2} - \mathbf{X}'_{\mathbf{F}_2}\right\|^2_{\mathbf{K}} \\ &= \left\|\mathbf{X}''_{\mathbf{F}_2} - \mathbf{X}_{\mathbf{F}_2}\right\|^2_{\mathbf{K}} + \left\|\mathbf{X}_{\mathbf{F}_2} - \mathbf{X}'_{\mathbf{F}_2}\right\|^2_{\mathbf{K}} - s\left\|\mathbf{X}_{\mathbf{F}_2} - \mathbf{X}'_{\mathbf{F}_2}\right\|^2_{\mathbf{N}} + s\left\|\mathbf{X}_{\mathbf{F}_2} - \mathbf{X}'_{\mathbf{F}_2}\right\|^2_{\mathbf{N}} \\ &= \left\|\mathbf{X}''_{\mathbf{F}_2} - \mathbf{X}_{\mathbf{F}_2}\right\|^2_{\mathbf{K}} + \left\|\mathbf{X}_{\mathbf{F}_2} - \mathbf{X}'_{\mathbf{F}_2}\right\|^2_{\mathbf{K}} \geq \left\|\mathbf{X}_{\mathbf{F}_2} - \mathbf{X}'_{\mathbf{F}_2}\right\|^2_{\mathbf{K}}\end{aligned} \tag{46}$$

with auxiliary solution $\mathbf{X}''_{\mathbf{F}_2}$ defined as:

$$\mathbf{X}''_{\mathbf{F}_2} = \mathbf{X}'_{\mathbf{F}_2} + sy_{2n,\mathbf{F}_2}\kappa_{2n,\mathbf{F}_2}\mathbf{u}_{2n+1,\mathbf{F}_2} \tag{47}$$

These error estimators of the approximations $\mathbf{X}''_{\mathbf{F}_1}$ and $\mathbf{X}''_{\mathbf{F}_2}$ can be used separately to control the error introduced by the reduction method. The number of stages of the equivalent circuit, i.e. the size of the reduced bases, can be tuned in order to achieve the desired accuracy.

Furthermore, the combined error estimator for $\mathbf{X}'_{\varphi} = \mathbf{X}'_{\mathbf{F}_1} + \mathbf{X}'_{\mathbf{F}_2}$ is given by:

$$\begin{aligned}\epsilon^2_{\mathbf{K}} &= \left\|\mathbf{X}''_{\mathbf{F}_1} + \mathbf{X}''_{\mathbf{F}_2} - \mathbf{X}'_{\mathbf{F}_1} - \mathbf{X}'_{\mathbf{F}_2}\right\|^2_{\mathbf{K}} \\ &= \left\|\mathbf{X}''_{\mathbf{F}_1} + \mathbf{X}''_{\mathbf{F}_2} - \mathbf{X}_{\varphi} + \mathbf{X}_{\varphi} - \mathbf{X}'_{\mathbf{F}_1} - \mathbf{X}'_{\mathbf{F}_2}\right\|^2_{\mathbf{K}} \\ &= \left\|\mathbf{X}''_{\mathbf{F}_1} + \mathbf{X}''_{\mathbf{F}_2} - \mathbf{X}_{\varphi}\right\|^2_{\mathbf{K}} + \left\|\mathbf{X}_{\varphi} - \mathbf{X}'_{\mathbf{F}_1} - \mathbf{X}'_{\mathbf{F}_2}\right\|^2_{\mathbf{K}} \geq \left\|\mathbf{X}_{\varphi} - \mathbf{X}'_{\mathbf{F}_1} - \mathbf{X}'_{\mathbf{F}_2}\right\|^2_{\mathbf{K}}\end{aligned} \tag{48}$$

The error on the approximation $\mathbf{X}_{\varphi}$ can be also easily obtained from the previous equation.

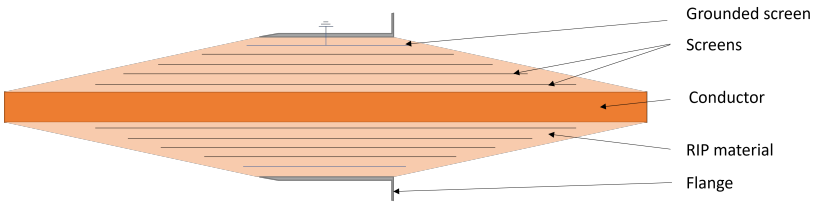

Figure 7: Schematic view of the bushing.

3. Application

To test the proposed method of reduction, we selected a resin-impregnated paper (RIP) transformer bushing as a case of study. Transformers are vital components of an electrical network, as they allow for transmitting electrical power from production to the load. Then, bushings are key equipment as they connect the winding of the transformer to the transmission cables, and are submitted to severe electromagnetic and environmental stress, such as high voltage, high temperatures and varying climatic conditions. A RIP bushing is made of crepe paper impregnated in resin, wrapped around a central conductor, with aluminum electrodes (screens) placed at carefully chosen positions to reduce the tangential component of the electric field, and a flange for grounding, as shown in Fig. 7.

According to [24], bushings are responsible for up to 60 percent of transformer failures, which often implies the complete destruction of the equipment due to fire damage. There are multiple causes of bushing failures that we can divide in three main categories: mechanical failure, thermal failure and insulation failure [25]. In this article, we focus on the latest type of failure, and more specifically on a common fault: the bridging of two capacitor screens (also referred as the loss of a capacitive layer), that can be caused by the deterioration of the insulating material or due to mistakes during the conception of the equipment.

In an industrial context, it is then crucial to prematurely detect such default before they become destructive for the bushing due to thermal stress. Thankfully, the degradation due to local modifications of the RIP material characteristics impacts global electrical quantities such as voltages and currents. These global quantities are much easier to measure than local quantities, therefore factors based on these global quantities are commonly used to evaluate the health of the device. In the following, we focus on a factor $\tan\delta(\omega)$, so-called the dissipation factor, defined by:

$$\tan\delta(\omega) = \frac{\frac{1}{R_c}}{\omega C_p} = \frac{\frac{V}{R_c}}{\omega C_p V} = \frac{I_R}{I_C} \tag{49}$$

$$I = I_R + jI_C \tag{50}$$

where V is the voltage applied to the bushing, which is assumed to be real, I is the current flowing through the bushing (see Fig. 8). This quantity represents the ratio between the resistive current I_R and the capacitive current I_C in the bushing, as shown on Fig. 9. As the bushing is essentially capacitive, this quantity is very small in healthy conditions in the considered frequency range [1mHz - 1kHz].

The RIP core is made of nine stratified layers, each separated by a fine capacitor screen which is made of a conductive material. These screens are assumed to be equipotential and are equipotential boundary conditions, denoted as $\Gamma_{E1}, \cdots, \Gamma_{E10}$. The potential of each screen is

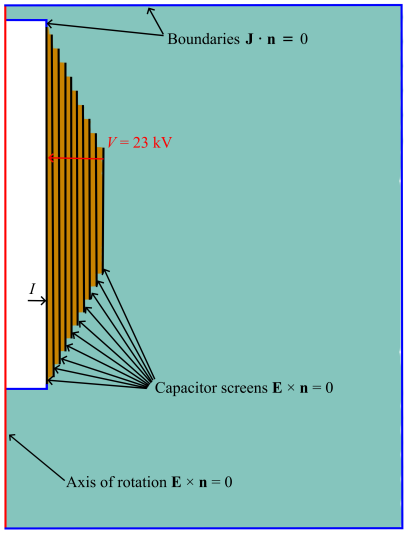

Figure 8: Illustration of the symmetry plane in the simulation domain for a healthy Bushing, highlighting the applied voltage source, the resulted current flow, and corresponding boundary conditions.

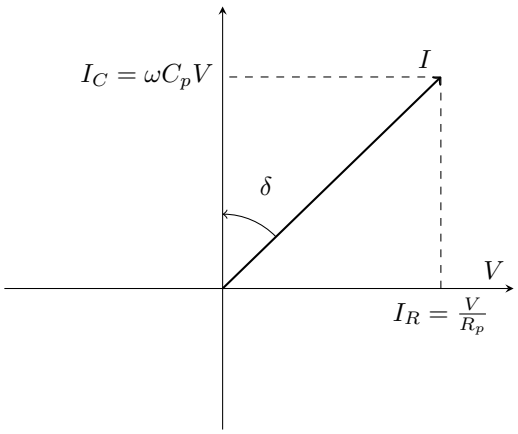

Figure 9: Calculation of the dissipation factor.

supposed to be floating and make up unknowns of the problem except the inner (Γ_{E1}) and the outer (Γ_{E10}) screens where the potential is imposed. These screens separate the different layers of the RIP core. Fig. 10 shows the configuration, showing the source and segmentation of different domains within the bushing's cross-section.

The material behavior law is assumed to be frequency-invariant and linear. The electrical conductivity and relative permittivity of the RIP are specified as 8.33×10^{-13} S/m and 2.19, respectively. Correspondingly, the air's conductivity and relative permittivity are 8.33×10^{-15} S/m and 1, respectively.

To evaluate the loss of a capacitive layer, we also simulate failure due to localized inter-screens insulation degradation. We choose to introduce the default between the eighth and ninth layers. The default is represented by a deteriorating channel connected to the capacitor screen as suggested by [26]. This channel is a cylinder with a diameter of 5.7 mm, which is depicted in Fig. 10. Under normal conditions, the channel's conductivity matches that of the RIP core; in the failure scenario, it increases to 8.33×10^{-6} S/m. The frequency range of analysis will be $[1 \times 10^{-3}, 1 \times 10^{3}]$ Hz. In healthy condition the problem is 2D however, in the faulty condition, the problem becomes 3D. The default is small compared to the whole structure of the bushing and leads to a local modification of the scalar potential and the electric field. The issue is then to evaluate if the proposed reduction method is able to capture a global behavior (healthy state) as well as local behavior (faulty state) and to see if we are able to calculate correctly the dissipation factor with the reduced model.

Subsequently, to compare the CLN method and the FE model, we will consider either global and local quantities. The global quantity will be the variation of the dissipation factor with the frequency. The local quantity will be the scalar potential and local electric field along the curve γ as shown in Fig. 11. The curve γ crosses the deteriorating channel and is perpendicular to the symmetry axis of the RIP core. Thus, the field along the curve is parameterized by the radial coordinate r. In the following, E_r is the component of the electric field in the radial direction in the cylindrical coordinate system.

The geometry is meshed with 135,345 tetrahedral elements. The total number of unknowns, which are the values of the scalar potential on the nodes of the mesh is equal to 9,265.

3.1. Healthy case

We consider first a healthy bushing. The evolution of the dissipation factor versus the frequency has been calculated using the FE model as shown in Fig. 12. We have applied the CLN method to construct a reduced model of the healthy bushing. We have considered a number of stages $n = 2$ and $n = 4$. When we look at the evolution of the dissipation factor calculating from the reduced model (see 12), the global characteristic is well captured using only two stages $n = 2$ of equivalent circuit, also depicted in Fig. 12. In the targeted frequency range, the bushing has a capacitive behavior. This is why it is easy to catch correctly the global behavior with only two stages and so to obtain good results for the dissipation factor.

Now if we look at the local behavior, the evolution of the real and imaginary parts of the scalar potential and the radial component of electric field E_r along the curve γ has been drawn for a frequency of 1 mHz and 1 kHz (Fig. 13 and Fig. 14). We can see that at high frequency (1 kHz), the local field distribution is adequately captured with only two stages. At low frequency, it appears that this is not the case and the relative error is high for imaginary parts. In fact, $n = 8$ is required to obtain equivalent results as the FE model (see Fig. 15).

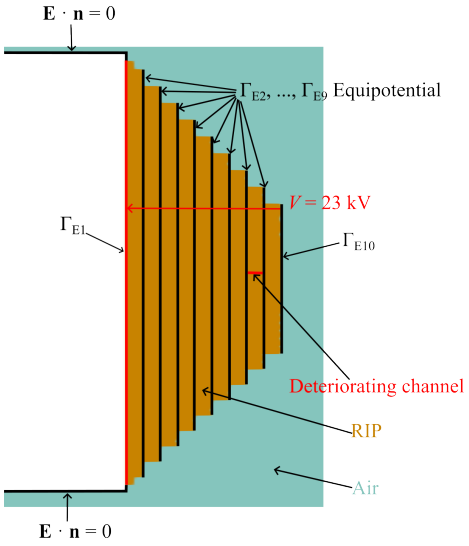

Figure 10: Cross-sectional view of the RIP bushing illustrating the layered structure, equipotential boundaries: $\Gamma_{E1}, \cdots, \Gamma_{E10}$ and the location of default.

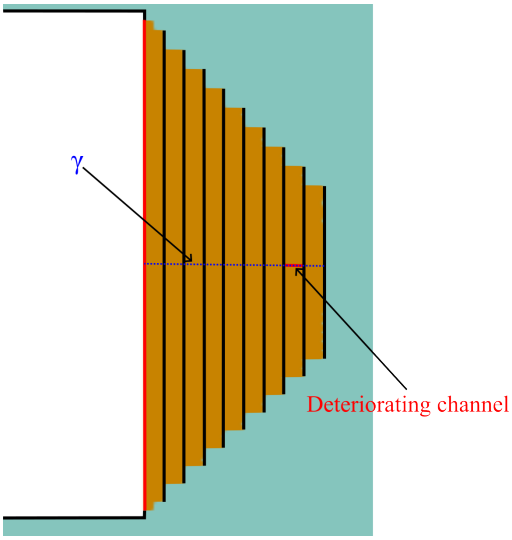

Figure 11: Illustration of the position of curve γ utilized for plotting the distribution of the local electric field.

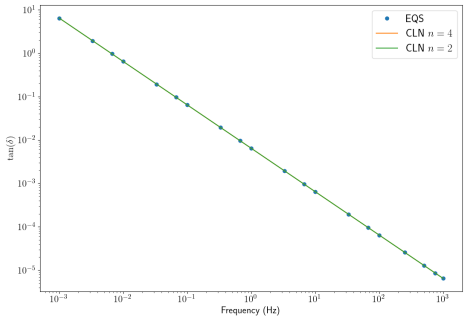

Figure 12: $\tan\delta(\omega)$ under healthy state obtained by the full model (EQS) and CLN with different stages ($n = 4$ and $n = 2$).

The CLN method is equivalent to a Padé approximation of transfer function $\mathcal{H}(s)$ at $s = 0$.

$$\mathcal{H}(s) = \mathbf{F}^t\mathbf{a} \tag{51}$$

In the MQS model, the CLN model is accurate at low frequency ($s = j\omega$). In the EQS case, due to the change of variable $s = 1/j\omega$, the CLN model is accurate at high frequency and the error discrepancy will appear firstly at low frequency, as it was illustrated with the results of simulation previously.

The evolution of the error estimator $\epsilon^2_{\mathbf{K}}$ defined in Eq. 48 in function of the frequency is presented in Fig. 16. Since we have access to the FE solution, considered as our reference model, we are also able to calculate $\epsilon^2_{\mathbf{K},\text{ex}} = \left\|\mathbf{X}''_{\mathbf{F}_1} + \mathbf{X}''_{\mathbf{F}_2} - \mathbf{X}_\varphi\right\|^2_{\mathbf{K}} + \left\|\mathbf{X}_\varphi - \mathbf{X}'_{\mathbf{F}_1} - \mathbf{X}'_{\mathbf{F}_2}\right\|^2_{\mathbf{K}}$, the right hand side of Eq. 48. We can see first that the error estimator enables to calculate a distance $\epsilon^2_{\mathbf{K}}$ with the FE solution without knowing it. At low frequencies, the error is relatively high, decreasing with an increase in frequency. Similarly, for a given frequency, the error decreases as the number of stages increases.

3.2. Default case

We now consider the bushing with a default as shown in Fig. 10. The evolution of the dissipation factor tan(δ) as a function of frequency has been calculated using the FE model, as shown in Fig. 17. It is observed that the default significantly influences the dissipation, especially for frequencies higher than 1 Hz. The dissipation factor seems to be a good candidate for local default detection like local conducting bridge between two screens.

We have applied the CLN method to construct a reduced model of the bushing with the default. The presence of the default increases the complexity of the problem which is now fully 3D. Consequently, more stages are required for the CLN model to accurately capture global characteristic (see Fig. 18). An increase in the number of stages also enhances the precision at low frequencies and we can see that with $n = 16$ the CLN model gives a frequency response for the dissipation factor very close to the FE model even at low frequency.

When examining the local behavior, the evolutions of both the real and imaginary parts of the scalar potential and the radial component of electric field along the curve γ have been shown for frequencies of 1 mHz and 1 kHz (refer to Fig. 19 and Fig. 20). It is observed that at a high frequency (1 kHz), the local field distribution is adequately captured with 16 stages. However, at

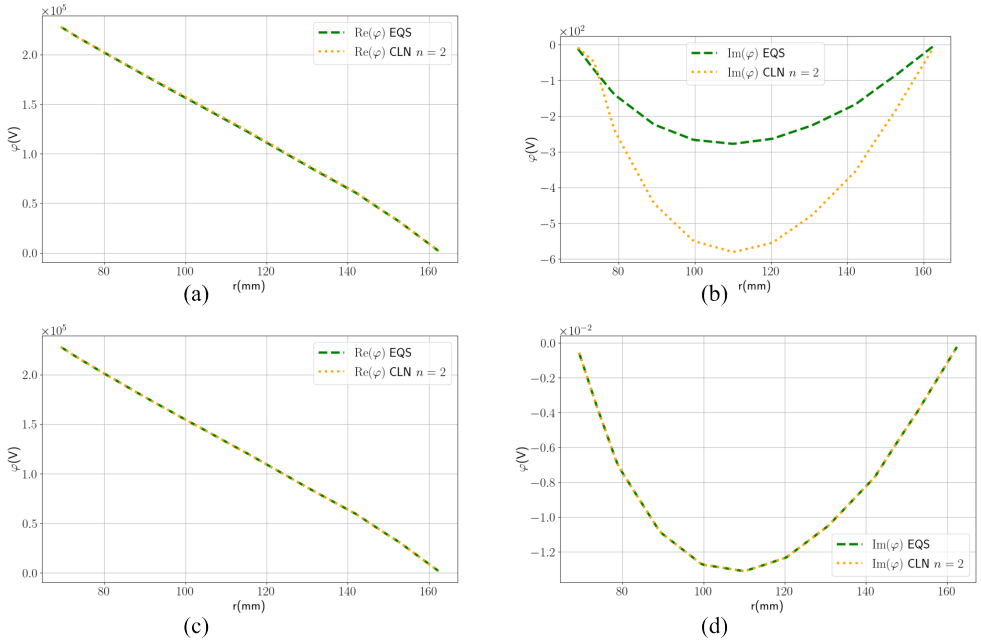

Figure 13: Under healthy state: (a) real part of the scalar potential (Re(φ)) for $f = 1$ mHz, (b) imaginary part of the scalar potential (Im(φ)) for $f = 1$ mHz, (c) real part of the scalar potential (Re(φ)) for $f = 1$ kHz, (d) imaginary part of the scalar potential (Im(φ)) $f = 1$ kHz.

low frequency, the precision is not as high, particularly for the imaginary parts, where the relative error is significant. In fact, $n = 24$ stages are required to achieve results equivalent to those of the FE model, as shown in Fig. 21.

The evolution of the error estimator as a function of frequency is presented in Fig. 22. As mentioned in the healthy case, since the CLN is equivalent to a Padé development at an infinite frequency we can see that the error due to the CLN approximation is decreasing in function of the frequency. It means that the error is the highest at low frequency. For the same frequency, we can verify also that the error decreases when increasing the number of stages. The results from the error estimator also explain the reduction in the error of the local field with an increasing number of stages, as depicted in Fig. 21.

In Table 1 presents the computational time for:

1. the FE model (T_{EQS}) to calculate 20 points in the frequency domain regularly distributed in the interval $[1 \times 10^{-3}, 1 \times 10^{3}]$ Hz.
2. the construction of CLN bases ($n = 16$) during the offline stage($T_{CLN,offline}$).
3. the CLN model during the online stage to calculate with the same point the frequency response of the bushing ($T_{CLN,online}$). Both equivalent electrical circuits have 16 stages leading to 32 state variables, which is 300 times smaller than the full problem.

We utilized MUMPS (MUltifrontal Massively Parallel sparse direct Solver) to solve the system of equations. We can see here that the computational time of the FE model is quite equivalent to the one of the CLN model accounting the offline stage. The CLN method achieved a real significant acceleration during the online stage. It enables if necessary to calculate new points in

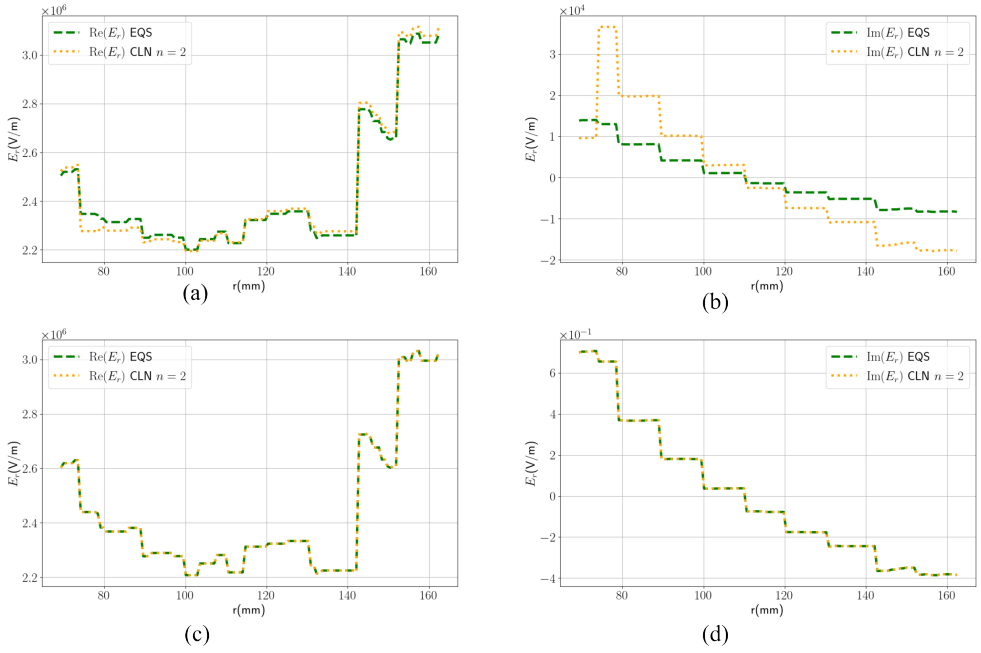

Figure 14: Under healthy state: (a) real part of the radial component of electric field E_r (Re(E_r)) for $f = 1$ mHz, (b) imaginary part of the radial component of electric field E_r (Im(E_r)) for $f = 1$ mHz, (c) real part of the radial component of electric field E_r (Re(E_r)) for $f = 1$ kHz, (d) imaginary part of the radial component of electric field E_r (Im(E_r)) $f = 1$ kHz.

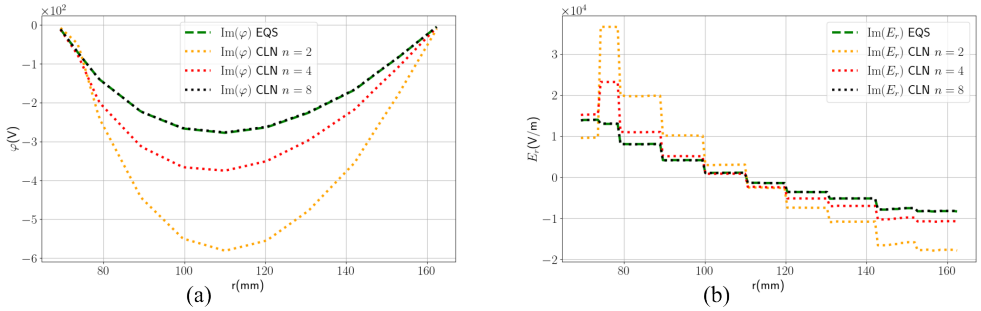

Figure 15: Under healthy state: (a) imaginary part of the scalar potential (Im(φ)) for $f = 1$ mHz obtained by EQS and CLN with $n = 2$, $n = 4$ and $n = 8$, (b) imaginary part of the radial component of electric field E_r (Im(E_r)) for $f = 1$ mHz obtained by EQS and CLN with $n = 2$, $n = 4$ and $n = 8$.

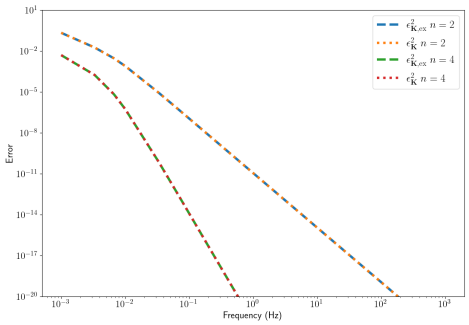

Figure 16: Comparison between the error estimator $\epsilon^2_{\mathbf{K}}$ and the exact error value $\epsilon^2_{\mathbf{K},\text{ex}}$ for a number of stages $n = 2$ and $n = 4$.

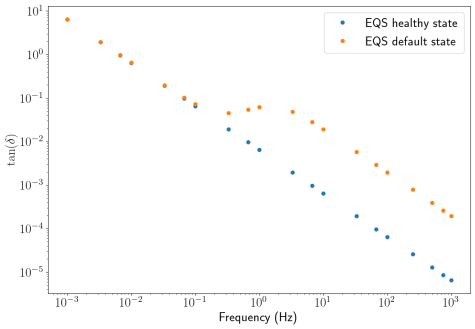

Figure 17: Comparison of $\tan\delta(\omega)$ under healthy state and faulty state.

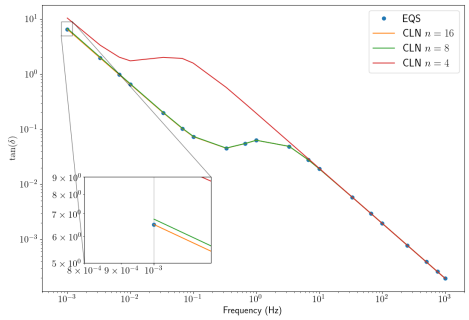

Figure 18: $\tan\delta(\omega)$ under faulty state obtain by full model (EQS) and CLN with different stages (n=16, n=8 and n=4).

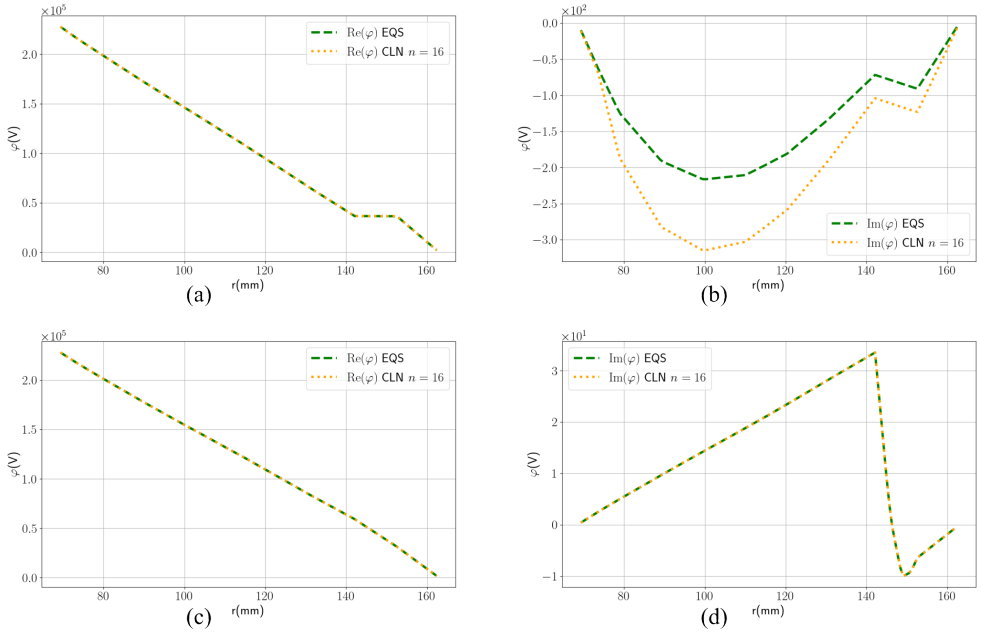

Figure 19: Under faulty state: (a) real part of the scalar potential (Re(φ)) for $f = 1$ mHz, (b) imaginary part of the scalar potential (Im(φ)) for $f = 1$ mHz, (c) real part of the scalar potential (Re(φ)) for $f = 1$ kHz, (d) imaginary part of the scalar potential (Im(φ)) $f = 1$ kHz.

T_{EQS} (s)	$T_{CLN,online}$ (s)	$T_{CLN,offline}$ (s)
13.6	2.63×10^{-4}	11.6

Table 1: Computational time with deterioration with $n = 16$.

the frequency if needed. In our case, it enables to calculate more points around 0 Hz where the variation of the dissipation is not linear anymore.

4. Conclusion

In this paper, the CLN method has been applied in order to construct a reduced model of an EQS FE model using the CLN method. It appears that the electro-quasistatic (EQS) problem should be divided into two linear systems of equations. The CLN method is then applied separately on each system leading to two equivalent electrical circuits. This method is equivalent to a Padé approximation at infinite frequency, distinguishing it from the standard CLN method applied for MQS problem. It generates two equivalent electrical circuits composed of resistances and capacitances. Once constructed, these equivalent circuits can approximate both global quantities and the local solution with significantly lower computational costs compared to the full model. The approximation error is quantifiable through an error estimator, which enables to determine the distance between the reduced solution obtained by the CLN method and the FE solution without solving the FE model.

We applied our method to a resin-impregnated paper transformer bushing in both healthy and faulty conditions. The global quantity, so-called dissipation factor, as well as the local field

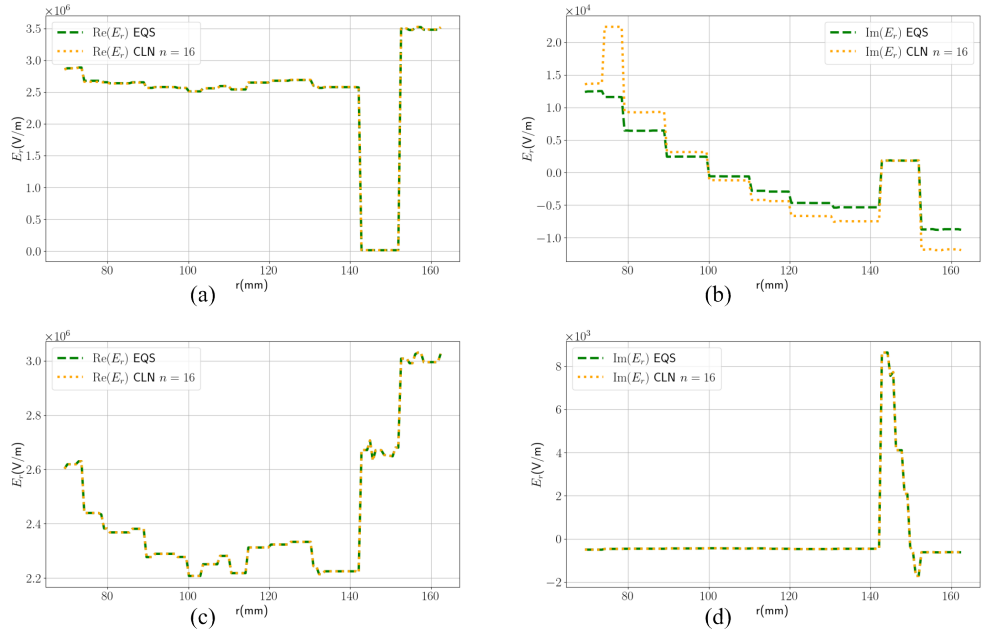

Figure 20: Under faulty state: (a) real part of the radial component of electric field E_r (Re(E_r)) for $f = 1$ mHz, (b) imaginary part of the radial component of electric field E_r (Im(E_r)) for $f = 1$ mHz, (c) real part of the radial component of electric field E_r (Re(E_r)) for $f = 1$ kHz, (d) imaginary part of the radial component of electric field E_r (Im(E_r)) $f = 1$ kHz.

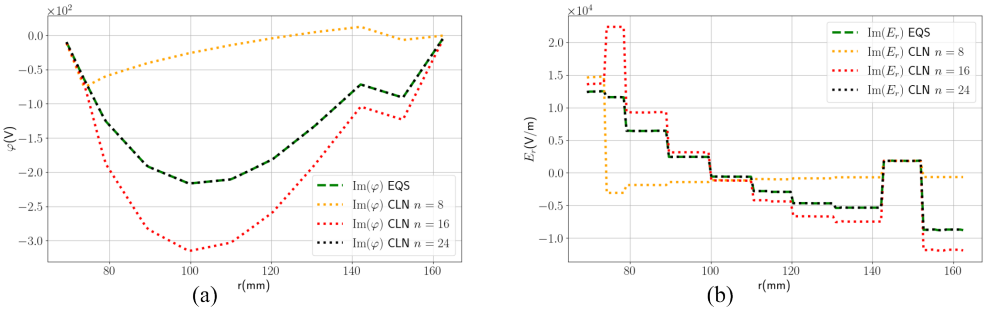

Figure 21: Under faulty state: (a) imaginary part of the scalar potential (Im(φ)) for $f = 1$ mHz obtained by EQS and CLN with $n = 8$, $n = 16$ and $n = 24$, (b) imaginary part of the radial component of electric field E_r (Im(E_r)) for $f = 1$ mHz obtained by EQS and CLN with $n = 8$, $n = 16$ and $n = 24$.

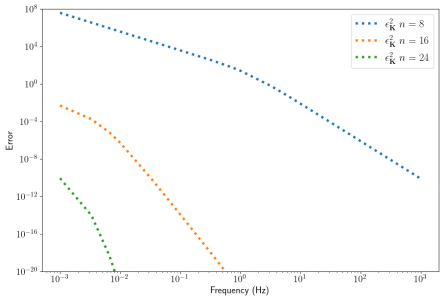

Figure 22: Comparison between the error estimator under faulty state obtain with different stages ($n = 8$, $n = 16$ and $n = 24$).

distribution in the whole frequency range, are accurately captured with only a few stages. Moreover, the accuracy of the local field approximation improves with an increased number of stages. Nevertheless, future research directions include the time domain estimator and extending the method's applicability to nonlinear cases and also accounting for several inputs using the multiport approach. Moreover, the CLN approach has been applied until now to MQS and EQS problems but it can be applied to other domains of physics, especially ones where equivalent electrical circuits are used like in thermal engineering for instance.

Acknowledgement

The authors gratefully acknowledge the financial support of the China Scholarship Council

CRediT authorship contribution statement

Wei Chen: Conceptualization, Methodology, Visualization, Writing - original draft
Thomas Henneron: Writing - Review & Editing, Supervision
Stéphane Clénet: Conceptualization, Methodology, Writing - original draft, Supervision
Théo Delagnes: Writing - Review & Editing, Resources
Jun Zou: Writing - Review & Editing, Supervision

Declaration of competing interest

The authors declare that they have no known competing financial interests or personal relationships that could have appeared to influence the work reported in this paper.

Data availability

The authors do not have the permission to share data

References

[1] J.-C. Nédélec, Mixed finite elements in $\mathbb{R}$ 3, Numerische Mathematik 35 (1980) 315–341.

[2] A. Bossavit, Computational electromagnetism and geometry: Building a finite-dimensional" Maxwell's house"-1-Network equations, Journal of the Japan Society of Applied Electromagnetics and Mechanics 7 (2) (1999) 150–159.

[3] A. Bossavit, Computational Electromagnetism: Variational Formulations, Complementarity, Edge Elements, Academic Press, 1998.

[4] M. Clemens, Large systems of equations in a discrete electromagnetism: Formulations and numerical algorithms, IEE Proceedings-Science, Measurement and Technology 152 (2) (2005) 50–72.

[5] Y. Späck-Leigsnering, E. Gjonaj, H. De Gersem, T. Weiland, M. Gießel, V. Hinrichsen, Electroquasistatic-thermal modeling and simulation of station class surge arresters, IEEE Transactions on Magnetics 52 (3) (2015) 1–4.

[6] J. L. Lumley, The structure of inhomogeneous turbulent flows, Atmospheric turbulence and radio wave propagation (1967) 166–178.

[7] L. Sirovich, Turbulence and the dynamics of coherent structures. I. Coherent structures, Quarterly of applied mathematics 45 (3) (1987) 561–571.

[8] D. Binion, X. Chen, A Krylov enhanced proper orthogonal decomposition method for efficient nonlinear model reduction, Finite Element in Analysis and Design 47 (7) (2011) 728–738. doi:10.1016/j.finel.2011.02.004.

[9] L. Jacques, E. Bechet, G. Kerschen, Finite element model reduction for space thermal analysis, Finite Element in Analysis and Design 127 (2017) 6–15. doi:10.1016/j.finel.2017.01.001.

[10] A. Odabasioglu, M. Celik, L. T. Pileggi, PRIMA: Passive reduced-order interconnect macromodeling algorithm, IEEE Transactions on computer-aided design of integrated circuits and systems 17 (8) (1998) 645–654.

[11] D. Binion, X. Chen, Coupled electrothermal-mechanical analysis for MEMS via model order reduction, FINITE ELEMENTS IN ANALYSIS AND DESIGN 46 (12) (2010) 1068–1076. doi:10.1016/j.finel.2010.07.007.

[12] F. Chinesta, A. Ammar, E. Cueto, On the use of proper generalized decompositions for multidimensional models, Revue européenne des éléments finis. Volume 8 (2) (2005).

[13] T. Henneron, S. Clenet, Separated representation of the finite element solution of nonlinear magnetostatic problem based on non-intrusive Proper Generalized, Finite Element in Analysis and Design 223 (2023) 103972. doi:10.1016/j.finel.2023.103972.

[14] M. Giacomini, L. Borchini, R. Sevilla, A. Huerta, Separated response surfaces for flows in parametrised domains: Comparison of a priori and a posteriori PGD algorithms, Finite Element in Analysis and Design 196 (2021) 103530. doi:10.1016/j.finel.2021.103530.

[15] A. Kameari, H. Ebrahimi, K. Sugahara, Y. Shindo, T. Matsuo, Cauer Ladder Network Representation of Eddy-Current Fields for Model Order Reduction Using Finite-Element Method, IEEE Transactions on Magnetics 54 (3) (Mar. 2018). doi:10.1109/TMAG.2017.2743224.

[16] S. Hiruma, H. Igarashi, Model Order Reduction for Linear Time-Invariant System With Symmetric Positive-Definite Matrices: Synthesis of Cauer-Equivalent Circuit, IEEE Transactions on Magnetics 56 (3) (2020) 1–8.

[17] N. Köster, O. König, O. Bíró, Proper Generalized Decomposition With Cauer Ladder Network Applied to Eddy Current Problems, IEEE Transactions on Magnetics 57 (6) (2021) 1–4.

[18] S. Hiruma, S. Clénet, H. Igarashi, Error Estimator for Continued Fraction Approximation of Linear Dynamical System, in: 2022 IEEE 20th Biennial Conference on Electromagnetic Field Computation (CEFC), 2022, pp. 1–2. doi:10.1109/CEFC55061.2022.9940814.

[19] D. Schmidthausler, M. Clemens, Low-order electroquasistatic field simulations based on proper orthogonal decomposition, IEEE Transactions on Magnetics 48 (2) (2012) 567–570.

[20] D. Schmidthäusler, S. Schöps, M. Clemens, Reduction of linear subdomains for non-linear electro-quasistatic field simulations, IEEE Transactions on Magnetics 49 (5) (2013) 1669–1672.

[21] C. Chi, Z. Ren, F. Yang, Model Order Reduction Based on Space-Harmonic Separation for Nonlinear Periodic EQS Problems, IEEE Transactions on Magnetics (2023) 1–1doi:10.1109/TMAG.2023.3324745.

[22] F. Kasolis, M. Clemens, Information-based model reduction for nonlinear electro-quasistatic problems, Journal of Computational Physics 404 (2020) 109118.

[23] Z. Ren, Influence of the RHS on the convergence behaviour of the curl-curl equation, IEEE Transactions on Magnetics 32 (3) (1996) 655–658. doi:10.1109/20.497323.

[24] S. M. Englund, Transformer bushing reliability, CIGRE, 2019.

[25] Z. Yuan, G. Sun, H. Tang, K. Gao, J. Hu, J. He, Types and Mechanisms of Condenser Transformer Bushing Failures, IEEE Electrical Insulation Magazine 39 (5) (2023) 26–36.

[26] M. Chen, X. Liu, P. Xu, T. Wen, Local Inter-foil Insulation Deterioration Diagnosis and Simulation of RIP Bushing Based on FDS Method, in: 2018 Condition Monitoring and Diagnosis (CMD), 2018, pp. 1–5. doi:10.1109/CMD.2018.8535656.